BIOCELL
2019 43(3): 207-213

Tech Science Press

SPAG9 promotes prostate cancer growth and metastasis

Chunhua YANG[1,2,3]; Ye TIAN[1,2,3]

[1] Department of Radiotherapy & Oncology, The Second Affiliated Hospital of Soochow University, Suzhou, China
[2] Institute of Radiotherapy & Oncology, Soochow University, Suzhou, China
[3] Suzhou Key Laboratory for Radiation Oncology, Suzhou, China

Key words: Angiogenesis, Bone metastasis, Invasion, Prostate cancer, SPAG9

Abstract: Sperm-associated antigen 9 (SPAG9) expression is increased in prostate tissues of prostate cancer patients. This experimental study aimed to investigate the role of SPAG9 in bone metastasis of prostate cancer. Immunohistochemical analysis showed that SPAG9 staining was positive in 81.67% of 240 cases of prostatic carcinoma but only in 6.67% of 120 cases of benign prostate hyperplasia. Strong PAG9 staining was positively correlated with Gleason score and bone metastasis in 240 prostate cancer patients ($p < 0.05$), but not with the age or serum prostate-specific antigen level ($p > 0.05$). PC-3 cells were transfected with shRNA against SPAG9, and CCK-8 assay in triplicate showed that PC-3 cell viability was inhibited by SPAG9 knockdown. In addition, transwell assay in triplicate showed that PC-3 cell invasion was inhibited by SPAG9 knockdown. Furthermore, total 2 × 106 PC-3 cells were injected subcutaneously into the right flank of nude mice which were randomly divided into three groups (N = 8) and treated by intratumoral injection of SPAG9 shRNA, control shRNA or PBS, respectively. SPAG9 shRNA inhibited the growth, invasion and angiogenesis while promoted apoptosis of xenografted PC-3 cells. SPAG9 knockdown led to the upregulation of E-cadherin and the downregulation of MMP2 and vimentin in xenografted tumors. In conclusion, this is the first study to provide evidence that SPAG9 promotes bone metastasis of prostate cancer, and SPAG9 is a promising target to prevent or treat bone metastasis of prostate cancer.

Introduction

Despite numerous diagnostic and therapeutic advances in recent years, prostate adenocarcinoma still has a high incidence in the Western population (Siegel *et al.*, 2017). Prostate cancer is prone to bone metastasis (Battafarano *et al.*, 2018). The incidence of bone metastasis is high in prostate cancer patients and their survival is only 12-53 months (Macedo *et al.*, 2017; Liu *et al.*, 2017).

Androgen deprivation therapy (ADT) is often used to decrease circulating testosterone levels by surgical or chemical castration (Dai *et al.*, 2017; Yap *et al.*, 2016). However, the response is transient and most patients will develop resistance to ADT and ultimately progress to castration-resistant prostate cancer (CRPC) (Wadosky *et al.*, 2016). For CRPC with bone metastasis, additional therapies have been approved recently, including targeted alpha therapy with radium-223 dichloride (Sumanasuriya *et al.*, 2017). However, the disease will ultimately relapse, indicating that effective therapy is needed to further improve the outcome.

Sperm-associated antigen 9 (SPAG9) emerges as a novel regulator of mitogen-activated protein kinases (MAPKs) pathway to modulate cancer growth and metastasis (Pan *et al.*, 2018). SPAG9 expression was increased in prostate cancer tissues (Chen *et al.*, 2014). However, the role of SPAG9 in bone metastasis of prostate cancer is unknown.

In this study, we hypothesized that SPAG9 promotes bone metastasis of prostate cancer and aimed to analyze the correlation of SPAG9 expression to bone metastasis and clinical pathological features of prostate cancer. Furthermore, we used highly metastatic PC-3 prostate cancer cell line to understand the mechanism by which SPAG9 promotes prostate cancer growth, angiogenesis, and invasion.

Materials and Methods

Immunohistochemistry

The protocols were approved by Institute Ethics Committee and all subjects provided informed consent. A total of 240 patients with prostate cancer (120 cases with bone metastasis and 120 cases without bone metastasis) were enrolled who underwent surgical resection at Second Affiliated Hospital of Soochow University between 2010 and 2017. 120 patients

*Address Correspondence to: Ye Tian,
yangchunhua820203@126.com

with benign prostate hyperplasia were enrolled as control. Clinical data were collected from their medical records. Only patients with confirmed diagnosis of prostate cancer or benign prostate hyperplasia by experienced urologists met the eligibility criteria and were included in the study groups, respectively. Immunohistochemical analysis of SPAG9 expression in clinical samples was performed as described previously (Chen *et al*., 2014). Briefly, tissue samples were fixed in paraformaldehyde, embedded and cut into 4 μm sections. Next, endogenous peroxidases were quenched and the sections were washed with 0.01 M phosphate buffered saline (PBS). The sections were blocked with 2% goat serum at room temperature for 1 h, then incubated with rabbit polyclonal anti-SPAG9 antibody (1:500 dilution, NB110-17780, Novus Biologicals, Littleton, CO, USA) at 4°C overnight, washed and then incubated with diaminobenzidine (Zhongshan Biotech, Beijing, China). For negative control, the sections were incubated with rabbit IgG serum. The stained sections were observed under microscope, and SPAG9 staining was scored by three pathologists independently in a blind manner based on the intensity and percentage of cells as follows: −, negative staining of almost all cells; +, weak staining of almost all cells; ++, moderate staining of more than 50% cells or strong staining of more than 5% cells; +++ strong staining of more than 50% cells. The correlation of SPAG9 staining with histopathological factors was analyzed by Pearson's test.

Cell culture

PC-3 prostate cancer cells were obtained from Institute of Biochemistry and Cell Biology, Chinese Academy of Sciences (Shanghai, China), and cultured in RPMI1640 medium (Gibco, USA) supplemented with 10% fetal calf serum (Gibco, USA), penicillin and streptomycin at 37°C in a humid incubator with 5% CO_2. Cells were passaged to maintain exponential growth, and only cells at exponential growth phase were used for further experiments. SPAG9 specific shRNA was constructed by GenePharma (Shanghai, China) and transfected into PC-3 cells using lipofectamin 2000 (Invitrogen, USA) according to the manufacturer's instructions. For negative control, cells were transfected with control shRNA.

Reverse transcription polymerase chain reaction (RT-PCR)

Total RNA was extracted from the cells using TRIzol reagent (Invitrogen, USA) following the manufacturer's protocols. cDNA was synthesized by reverse transcription using Access RT-PCR System (Promega, Madison, WI, USA). Real-time PCR was performed using SYBR Green PCR Master Mix (Applied Biosystems) on ABI Prism 7700 Sequence Detection System (Applied Biosystems) with the following primers: SPAG9 5'-AGAGGAAGGCTTGGGAGTA-3' and 5'-GGGCAGCAGAGCTATGTG-3'. The reaction conditions were 40 cycles at 94°C for 1 min, 50°C for 1 min and 68°C for 1 min. PCR was performed three times in triplicate, and relative mRNA levels of SPAG9 were calculated by $2^{-\Delta\Delta Ct}$ method.

Western blot analysis

Cells were collected by centrifugation and lysed in RIPA lysis buffer (Santa Cruz Biotechnology, USA). Equal amounts of proteins in cell lysates were separated by SDS-PAGE and transferred to nitrocellulose membranes. The membranes were incubated with SPAG9 or β-actin antibody (Santa Cruz Biotechnology, USA) at 4°C overnight, and then with secondary antibodies (Santa Cruz Biotechnology, USA) at room temperature for 1 h. The membranes were developed by using ECL kit (Pierce, USA) and the bands were quantitated by an image analyzer (LabWorks, Upland, CA, USA) with β-actin as loading control.

Cell proliferation assay

The proliferation of PC-3 cells was evaluated by CCK-8 method as described previously (Zhong *et al*., 2018). Briefly, the cells were seeded into 96-well plates. After culture at 37°C in a humid incubator with 5% CO_2 for 48 h, 10 μL CCK-8 solution (Sigma, USA) was added into each well and after incubation for 1 h, the OD at 450 nm was measured by a microplate reader.

In vitro invasion assay

The invasion of PC-3 cells was evaluated by transwell chamber as described previously (Tian *et al*., 2017). Briefly, 10^5 cells in serum-free medium were loaded into the upper chamber while 10% FBS were loaded into the lower chamber. After incubation at 37°C in a humid incubator with 5% CO_2 for 20 h, the cells on the top of the filters were removed by cotton swab. The remaining cells were fixed in 4% paraformaldehyde, stained with Crystal Violet and stained cells were counted in five randomly selected fields. At least three chambers from three different experiments were analyzed.

Xenograft tumor model in nude mice

Animal study protocols were approved by Institutional Animal Care and Use Committee. BALB/c nude mice (4-5 weeks old) were obtained from Experimental Animal Center of the Chinese Academy of Sciences (Shanghai, China). Total 2×10^6 PC-3 cells were injected subcutaneously into the right flank of mice. When tumors grew to about 100 mm^3, the mice were randomly divided into three groups (N = 8) and were treated by intratumoral injection of SPAG9 shRNA, control shRNA vectors (all constructed by GenePharma, Shanghai, China) or PBS, respectively. Tumor volume was calculated as: V (mm^3) = length of tumor x width of $tumor^2$/2. At the end, tumor tissues were dissected and apoptotic cells were detected by TUNEL assay using in situ apoptosis detection kit (Roche, Indianapolis, IN, USA) following the manufacturer's protocols.

Statistical analysis

Statistical analysis was performed using Student's t test for the comparison between two groups or analysis of variance (ANOVA) test followed by Tukey's test for the comparison among multiple groups. $p < 0.05$ was considered to be significant.

Results

Correlation of SPAG9 expression with clinicopathological factors in prostate cancer patients

By immunohistochemical analysis, SPAG9 staining was positive in 81.67% of 240 cases of prostatic carcinoma but was only 6.67% in 120 cases of benign prostate hyperplasia. SPAG9 staining was dominant in the nucleus (Fig. 1). Strong PAG9 staining was positively correlated with Gleason score and bone metastasis ($P < 0.05$), but not with the age or serum prostate-specific antigen level ($P > 0.05$) (Tab. 1).

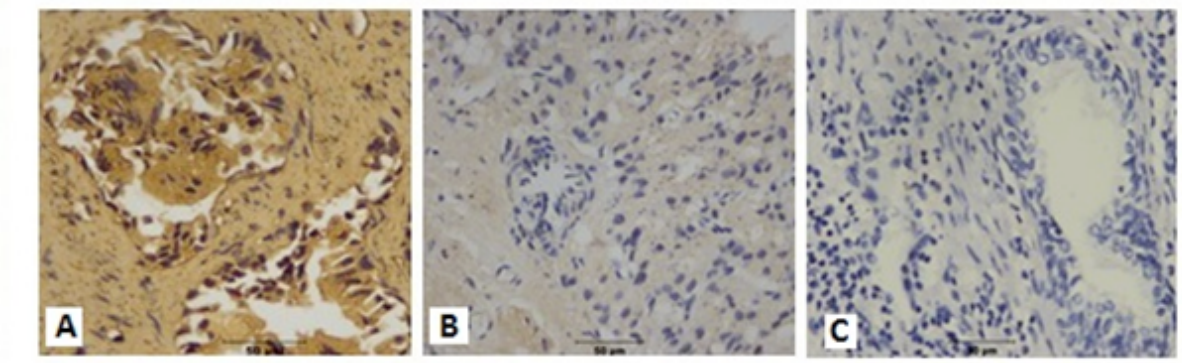

FIGURE 1. SPAG9 immunohistochemical staining. (A) prostate cancer with bone metastasis. (B) prostate cancer without bone metastasis. (C) benign prostate hyperplasia. Amplification: 400x.

TABLE 1

SPAG9 expression with clinicopathologic factors

factor	cases	SPAG9 expression(cases)				*p*-value (rank test)	*p*-value (Spearman rank correlation analysis)
		-	+	++	+++		
Age (year)							
≤ 70	120	20	24	48	28		
> 70	120	24	32	40	24	0.518	0.522
PSA (ng/ml)							
≤ 20	60	8	16	24	12		
> 20	180	36	40	64	40	0.821	0.868
Gleason score							
≤ 7	148	40	36	52	20		
> 7	92	4	20	36	32	0.013*	0.011**
metastases							
-	120	32	40	32	16		
+	120	12	16	56	36	0.007**	0.006**

SPAG9 knockdown inhibited prostate cancer growth and invasion

To explore the mechanism by which SPAG9 promotes bone metastasis of prostate cancer, we selected highly metastatic PC-3 prostate cancer cell line as in vitro cell model. We transfected pGPU6/GFP/Neo-SPAG9 into PC-3 cells to knockdown SPAG9 (Fig. 2(A)). CCK-8 assay showed that PC-3 cell viability was inhibited at 0.96 ± 0.05, 1.27 ± 0.08, and 1.39 ± 0.07, respectively, at 48, 72, 96 h after transfection of pGPU6/GFP/Neo-SPAG9 (Fig. 2(B)). In addition, transwell assay showed that the number of invaded PC-3 cells was 174.4 ± 9.7 after PBS treatment, 168.9 ± 8.9 after transfection with pGPU6/GFP/Neo, and 90.3 ± 6.7 after transfection with pGPU6/GFP/Neo-SPAG9 (Fig. 2(C)).

Furthermore, *in vivo* nude mice model showed that final volume of tumors was 339.1 ± 13.1 mm^3, 569.3 ± 31.1 mm^3, and 574.8 ± 41.1 mm^3 in pGPU6/GFP/Neo-SPAG9, pGPU6/GFP/Neo and PBS group, respectively (Fig. 3(A)). Western blot analysis confirmed SPAG9 knockdown in nude mice that received pGPU6/GFP/Neo-SPAG9 (Fig. 3(B)). In addition, immunohistochemical analysis showed low SPAG9 expression in nude mice that received pGPU6/GFP/Neo-SPAG9 (Fig. 3(C)).

HE-staining of the tumors showed that in pGPU6/GFP/Neo group and PBS group, tumor cells were dense with irregular shape and intact nuclei. In contrast, in pGPU6/GFP/Neo-SPAG9 group, we observed many dead cells within the tumor tissue with fractured nucleus pyknosis (Fig. 4(A)). Furthermore, TUNEL assay showed higher percentage of apoptotic cells in pGPU6/GFP/Neo-SPAG9 group (67.63 ± 6.24%) than in pGPU6/GFP/Neo group (31.84 ± 2.135) and PBS group (30.44 ± 3.41%) ($p < 0.01$) (Figs. 4(B)-4(C)).

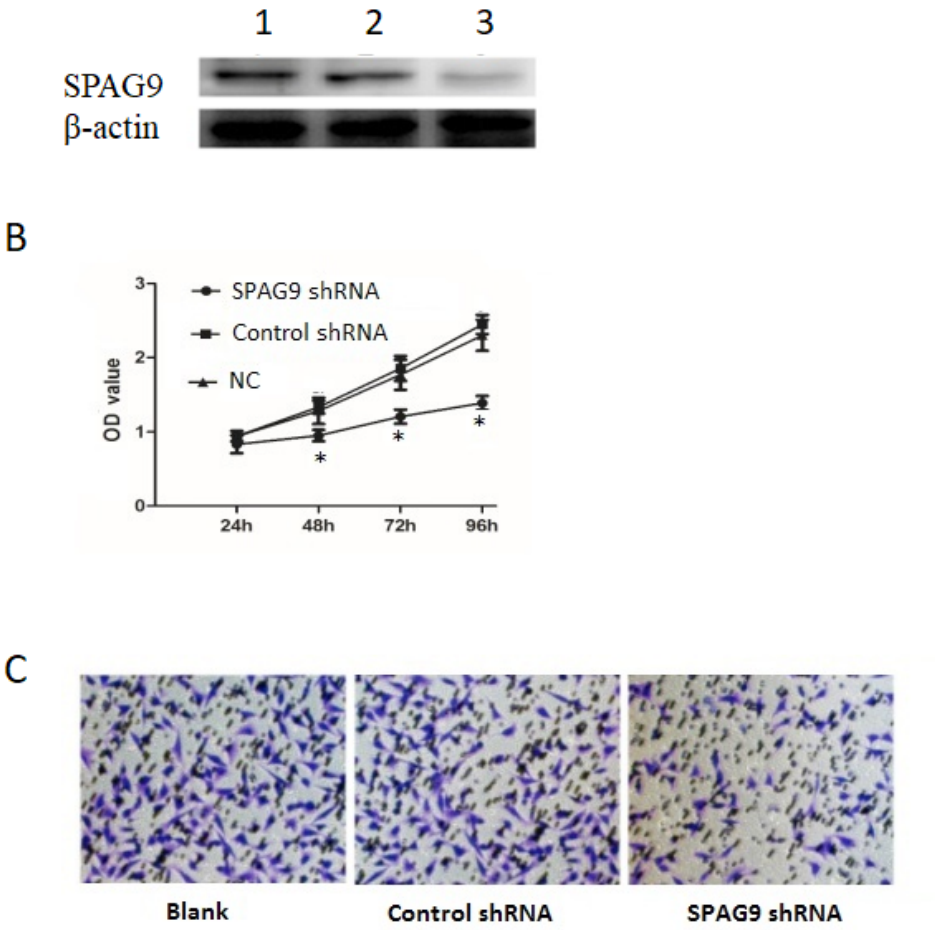

FIGURE 2. SPAG9 knockdown inhibited the proliferation and invasion of PC-3 cells. (A) Western blot analysis of SPAG9 protein levels. 1. PBS group. 2. Control shRNA group. 3. SPAG9 shRNA group. (B) CCK8 assay of the proliferation of PC-3 cells (N = 3). * $p < 0.05$ compared with the control groups. (C) Transwell assay of the invasion of PC-3 cells.

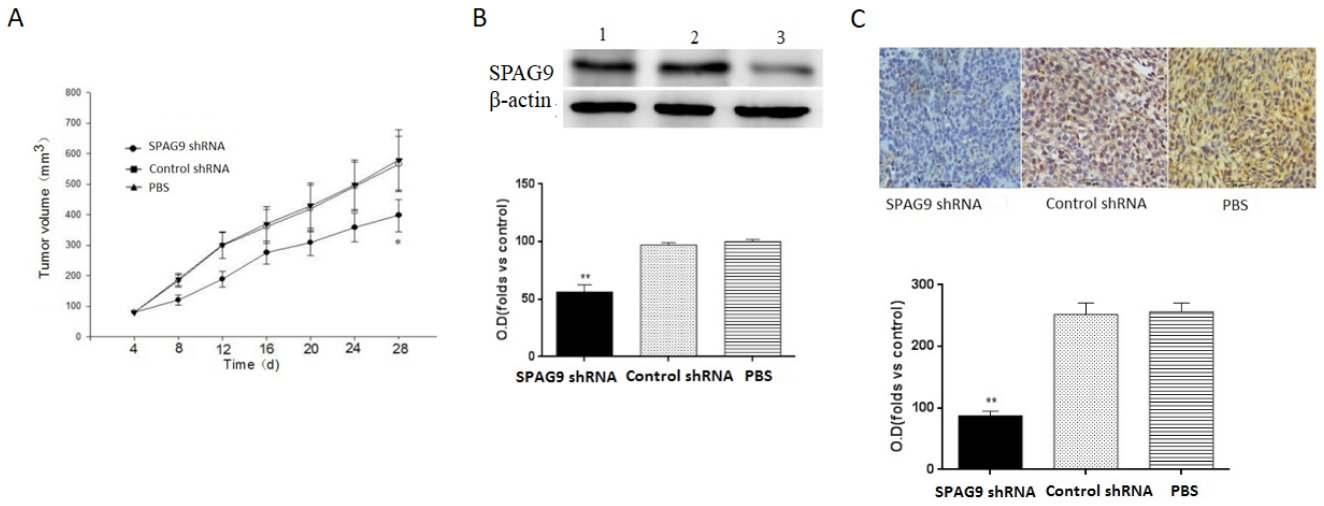

FIGURE 3. SPAG9 knockdown inhibited the growth of xenografts from PC-3 cells. (A) Tumor growth curve of each group (N = 8). * $p < 0.05$ *vs.* control groups. (B) Western blot analysis of SPAG9 protein levels in xenografts. 1. PBS group. 2. Control shRNA group. 3. SPAG9 shRNA group. (C) Immunohistochemical staining of SPAG9 in xenografts. Amplification: 400x. ** $p < 0.01$ *vs.* control shRNA group and PBS group (N = 3).

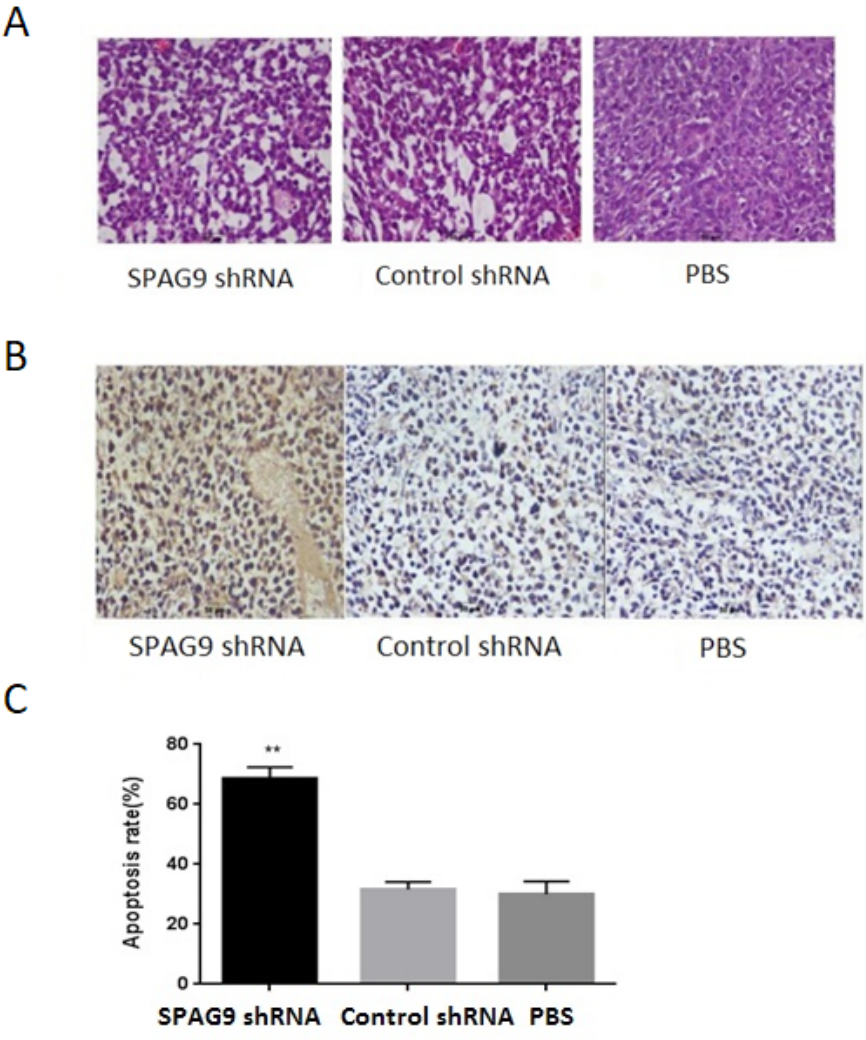

FIGURE 4. SPAG9 knockdown induced apoptosis in xenografts from PC-3 cells. (A) HE-staining of xenografts. Amplification: 400x. (B) TUNEL assay of apoptotic cells in xenografts. Amplification: 400x. (C) Quantitative analysis of apoptotic cells (N = 3). ** $p < 0.01$ *vs.* other groups.

SPAG9 regulates the invasion and angiogenesis of xenografted prostate cancer

Immunohistochermical staining of Vimentin and MMP2 in pGPU6/GFP/Neo-SPAG9 group (75.87 ± 6.89, 74.79 ± 8.12, respectively) was weaker than in pGPU6/GFP/Neo group (154.20 ± 10.31, 175.82 ± 10.57, respectively) and PBS group (151.69 ± 12.96, 182.17 ± 9.59, respectively), but the staining intensity of E-cadherin in pGPU6/GFP/Neo-SPAG9 group (306.13 ± 21.87) was higher than in pGPU6/GFP/Neo group (166.92 ± 17.90) and PBS group (158.92 ± 16.73) ($p < 0.01$, Figs. 5(A)-5(B)).

In addition, the staining intensity of CD31, a marker of angiogenesis, was 91.49 ± 5.29, 168.37 ± 8.99 and 172.98 ± 15.70 in pGPU6/GFP/Neo-SPAG9 group, pGPU6/GFP/Neo group and PBS group, respectively. CD31 protein expression was significantly lower after SPAG9 knockdown compared to the controls ($p < 0.01$, Figs. 5(C)-5(D)).

Discussion

To our knowledge, this is the first study to report that SPAG9 expression in prostate cancer showed a positive correlation with Glean score and bone metastasis, suggesting that SPAG9 may play a role in bone metastasis of prostate cancer and could be a therapy target for prostate cancer. However, due to limited data, potential bias of correlation analysis may be overlooked and need to be further addressed in future clinical studies.

In present study, we silenced SPAG9 expression with shRNA and found that SPAG9 knockdown inhibited the viability and invasion of PC-3 cells. Our results are in agreement with previous findings that SPAG9 knockdown and SPAG9 overexpression decreased and increased cancer cell proliferation, respectively (Li *et al.*, 2014).

To further elucidate the mechanism by which SPAG9 promotes prostatic carcinoma progression and metastasis *in vivo*, we focused on EMT markers such as E-cadherin and vimentin (Tanaka *et al.*, 2013). We found that SPAG9 knockdown led to decreased expression of vimentin and MMP2 and increased expression of E-cadherin. These data indicate that SPAG9 enhances EMT to promote prostate cancer metastasis.

Angiogenesis is essential to tumor metastasis (Wu *et al.*, 2018). SPAG9 could regulate JNK pathway and JNK induces the activation of VEGF (Garg *et al.*, 2008; Guma *et al.*, 2009). Thus, SPAG9 may promote cancer angiogenesis via JNK signaling. In our study, we found that the well-known marker of angiogenesis CD31 was downregulated in pGPU6/GFP/Neo-SPAG9 group. Thus, SPAG9 knockdown inhibited the formation of blood vessels. Moreover, SPAG9 knockdown induced apoptosis in prostate cancer cells xenografted into nude mice.

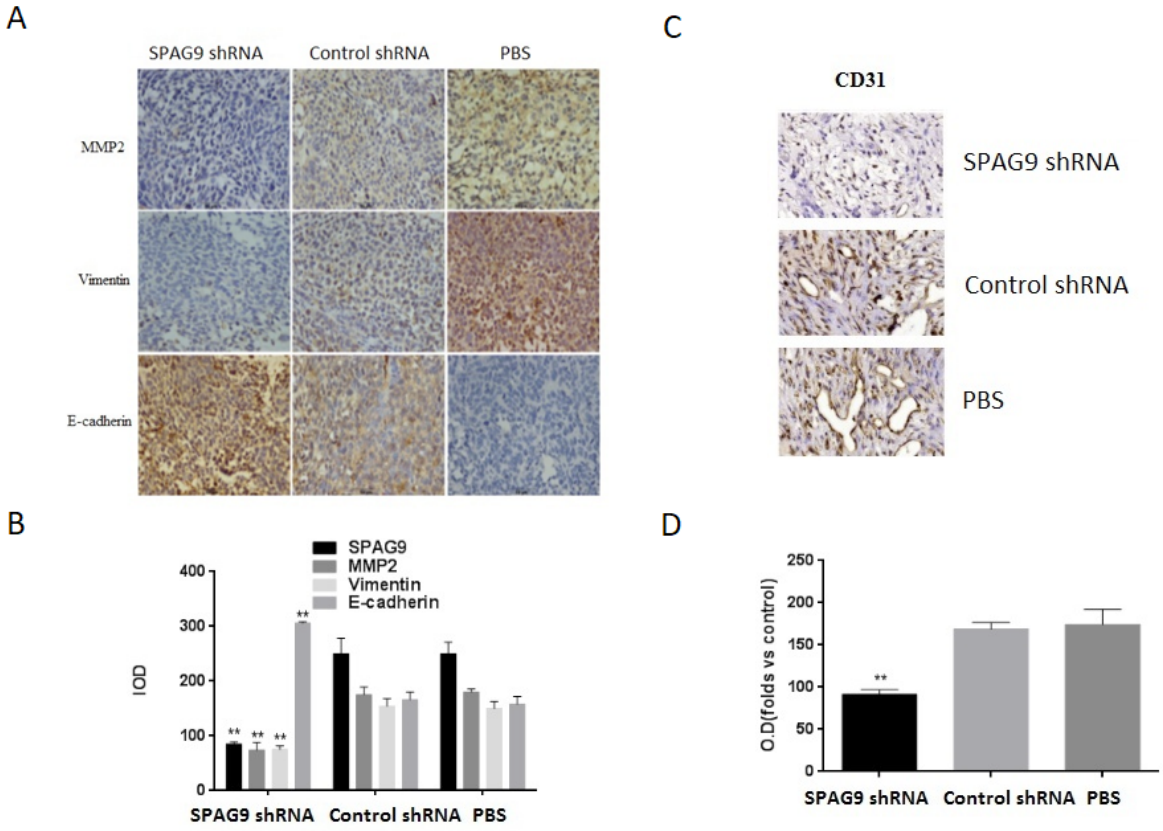

FIGURE 5. SPAG9 knockdown regulated the expression of metastasis and angiogenesis related proteins in xenografts from PC-3 cells. (A) Immunohistochemistry analysis of vimentin, MMP2 and E-cadherin in xenografts. Amplification: 400x. (B) Staining intensity of vimentin, MMP2 and E-cadherin (N = 3). ** $p < 0.01$ *vs.* other groups. (C) Immunohistochemistry analysis of CD31 in xenografts. Amplification: 400x. (D) Staining intensity of CD31 (N = 3). ** $p < 0.01$ *vs.* other groups.

Taken together, SPAG9 expression is high in prostate cancer tissues and is positively correlated with Glean score and bone metastasis. Silencing SPAG9 could inhibit the growth, invasion and angiogenesis while promote apoptosis of xenografted PC-3 cells. These findings suggest that SPAG9 promotes the occurrence and bone metastasis of prostate cancer, and further studies are needed to confirm that SPAG9 is a promising target to prevent or treat bone metastasis of prostate cancer.

References

Battafarano G, Rossi M, Marampon F, Del Fattore A (2018). Cellular and molecular mediators of bone metastatic lesions. *International Journal of Molecular Sciences* **19**: 6.

Chen F, Lu Z, Deng J, Han X, Bai J, Liu Q, Xi Y, Zheng J (2014). SPAG9 expression is increased in human prostate cancer and promotes cell motility, invasion and angiogenesis in vitro. *Oncology Reports* **32**: 2533-2540.

Dai C, Heemers H, Sharifi N (2017). Androgen signaling in prostate cancer. *Cold Spring Harbor Perspectives in Medicine* **7**: a030452.

Garg M, Kanojia D, Khosla A, Dudha N, Sati S, Chaurasiya D, Jagadish N, Seth A, Kumar R, Gupta S, Gupta A, Lohiya NK, Suri A (2008). Sperm-associated antigen 9 is associated with tumor growth, migration, and invasion in renal cell carcinoma. *Cancer Research* **68**: 8240-8248.

Guma M, Rius J, Duong-Polk KX, Haddad GG, Lindsey JD, Karin M (2009). Genetic and pharmacological inhibition of JNK ameliorates hypoxia-induced retinopathy through interference with VEGF expression. *Proceedings of the National Academy of Sciences of the United States of America* **106**: 8760-8765.

Li H, Peng Y, Niu H, Wu B, Zhang Y, Zhang Y, Bai X, He P (2014). SPAG9 is overexpressed in human prostate cancer and promotes cancer cell proliferation. *Tumor Biology* **35**: 6949-6954.

Liu M, Zhang X (2017). An integrated analysis of mRNA-miRNA transcriptome data revealed hub regulatory networks in three genitourinary cancers. *Biocell* **41**: 19-26.

Macedo F, Ladeira K, Pinho F, Saraiva N, Bonito N, Pinto L, Goncalves F (2017). Bone metastases: an overview. *Oncology Reviews* **11**: 321.

Pan J, Yu H, Guo Z, Liu Q, Ding M, Xu K, Mao L (2018). Emerging role of sperm-associated antigen 9 in tumorigenesis. *Biomedicine & Pharmacotherapy* **103**: 1212-1216.

Siegel RL, Miller KD, Jemal A (2017). Cancer statistics. *CA: A Cancer Journal for Clinicians* **67**: 7-30.

Sumanasuriya S, de Bono J (2017). Treatment of advanced prostate cancer-A review of current therapies and future promise. *Cold Spring Harbor Perspectives in Medicine* **8**: a030635.

Tanaka Y, Terai Y, Kawaguchi H, Fujiwara S, Yoo S, Tsunetoh S, Takai M, Kanemura M, Tanabe A, Ohmichi M (2013). Prognostic impact of EMT (epithelial-mesenchymal-transition) related protein expression in endometrial cancer. *Cancer Biology & Therapy* **14**: 13-19.

Tian H, Cong P, Qi R, Gao X, Liu X, Liu H. Shan F (2017). Decreased invasion ability of hypotaurine synthesis deficient glioma cells was partially due to hypomethylation of Wnt5a promoter. *Biocell* **41**: 27-32.

Wadosky KM, Koochekpour S (2016). Molecular mechanisms underlying resistance to androgen deprivation therapy in prostate cancer. *Oncotarget* **7**: 64447-64470.

Wu T, Ding X, Su B, Soodeen-Lalloo AK, Zhang L, Shi JY (2018). Magnetic resonance imaging of tumor angiogenesis using dual-targeting RGD10-NGR9 ultrasmall superparamagnetic iron oxide nanoparticles. *Clinical & Translational Oncology* **20**: 599-606.

Yap TA, Smith AD, Ferraldeschi R, Al-Lazikani B, Workman P, de Bono JS (2016). Drug discovery in advanced prostate cancer: Translating biology into therapy. *Nature Reviews. Drug Discovery* **15**: 699-718.

Zhong J, Deng L, Jiang Y, Zou L, Yuan H, Tan S (2018). Gene expression profiling of $HepG_2$ cells after treatment with black tea polyphenols. *Biocell* **42**: 99-104.